Interannual variability of the 12-hour tide in the mesosphere and lower thermosphere in 15 years of meteor-radar observations above Rothera (68°S, 68°W)

Shaun M. Dempsey[1,2]**,Phoebe E. Noble**[1,2]**,Corwin J. Wright**[1]**,Tracy Moffat-Grffin**[2]**,Nicholas J. Mitchell**[2,1]

[1]Centre for Atmospheric and Oceanic Sciences, Department of Electronic and Electrical Engineering, University of Bath, Bath, UK
[2]British Antarctic Survey, Cambridge, UK

Key Points:

- Large amplitude tides are present in the mesosphere and lower thermosphere
- There is considerable interannual variability in monthly 12-hour tidal amplitudes
- The climate indices F10.7, QBO10, QBO30 and SAM all display significant correlations with variability in the tidal amplitudes

Corresponding author: Shaun M. Dempsey, `smd62@bath.ac.uk`

Abstract

The tides of the mesosphere and lower thermosphere (MLT) show great variability on timescales of days to years, with significant variability at interannual timescales. However, the nature and causes of this variability remain poorly understood. Here, we present measurements made over the interval 2005 to 2020 of the interannual variability of the 12-hour tide as measured at heights of 80 to 100 km by a meteor radar over the British Antarctic Survey base at Rothera (68°S, 68°W). We use a linear regression analysis to investigate correlations between the 12-hour tidal amplitudes and several climate indices, specifically the solar cycle (as measured by F10.7 solar flux), El Niño Southern Oscillation (ENSO), the Quasi-Biennial Oscillation (QBO) at 10 hPa and 30 hPa, the Southern Annular Mode (SAM) and investigate any linear trends. Our observations reveal that the 12-hour tide has a large amplitude and a clearly defined seasonal cycle with monthly mean values as large as 35 ms^{-1}. We observe substantial interannual variability, exhibiting an interdecile range in monthly mean tidal amplitudes at the height of 95 km in spring of 17.2 ms^{-1}, 12.6 ms^{-1} in summer, 23.6 ms^{-1} in autumn and 9.0 ms^{-1} in winter. We find that F10.7, QBO10, QBO30, SAM and time all have significant correlations at the 95% level, whereas we detect very minimal correlation with ENSO. These results suggest that variations in F10.7, the QBO and SAM may contribute significantly to the interannual variability of tidal amplitudes in the Antarctic MLT.

1 Introduction

In the mesosphere and lower thermosphere (MLT), from heights of 80 to 100 km, the wind field is dominated by global scale oscillations; atmospheric tides. The tides in the MLT have very large amplitudes and hence are critical to the dynamics of the whole atmosphere. Therefore, tides are vital to understanding it in its entirety (Smith, 2012). These tides are created by the solar heating of ozone and water vapour in the troposphere and stratosphere, the release of latent heat in deep tropospheric convection, or planetary-scale non-linear interactions. The tides are apparent in many different atmospheric variables such as wind, temperature, airglow, and density.

Meteor radar observations of the MLT winds reveal large amplitude tides with periods equal to integer fractions of the solar day. At polar latitudes, the largest amplitudes are observed in the 12-hour tide, followed by the 24-hour tide (Dempsey et al., 2021; Davis et al., 2013). Higher frequency tides are also present, such as the 8-hour tide; however, these typically have much lower amplitudes. Conversely, at low latitudes, the 24-hour tide generally has larger amplitudes (Mitchell, 2002; Davis et al., 2013). We observe the tides as a superposition of two components; migrating and non-migrating. The migrating components are sun-syncronous (i.e. they follow the sun) and propagate westward. Conversely, the non-migrating components are not sun-following and are believed to be created primarily by the non-linear interactions between the migrating tides and planetary waves, generating the so-called secondary waves, including these non-migrating modes.

These oscillations are the most prominent features of the wind field of the MLT. Consequently, they have a profound impact on the dynamics of the atmosphere, both directly and indirectly. For example, tidal winds can filter the field of atmospheric gravity waves. This filtering controls the propagation of gravity waves to greater heights by modulating gravity wave momentum fluxes and the resulting forcing of the global atmospheric circulation (Fritts & Alexander, 2003; Yiğit et al., 2021). Tidal temperature perturbations, in addition to wind perturbations, are thought to be a fundamental driver of the variability of polar mesospheric clouds because they can modulate the cloud ice crystal population (Fiedler et al., 2005). Tidal signatures propagate upwards from the MLT into the thermosphere. They can perturb neutral and plasma densities in the E and F regions of the ionosphere, modulating the ionospheric wind dynamo and the distribution of ionisation in the ionosphere (Yiğit & Medvedev, 2015).

In this study, using meteor radar observations of the MLT, we assess the role of large-scale climate processes in controlling tides in the MLT at high latitudes and attempt to identify any correlations between climate indices and 12-hour monthly tidal amplitudes via a linear regression model. This will allow us to find any previously unknown connections. The processes we study (e.g. solar flux, ENSO, QBO and SAM) are known to have broad-scale impacts on tropospheric and stratospheric atmospheric processes, but their contribution to the dynamics of mesospheric tides is poorly quantified and understood. We use meteor radar to measure winds in the MLT and calculate monthly tidal amplitudes. Ground-based meteor radars have an excellent time and height resolution, and this dataset allows us to use this excellent resolution over the fifteen-year time series.

Many tidal studies have used ground-based measurements, such as meteor radar (e.g. Stober, Kuchar, et al. (2021); Dempsey et al. (2021); Davis et al. (2013); C. Beldon et al. (2006); Mitchell (2002)). Meteor radars provide excellent height and time resolution and are able to determine tidal amplitudes, wavelengths, and variability at all scales. They can produce reliable measurements at heights from 80 to 100 km, where tidal modes reach substantial amplitudes, unlike other ground-based techniques, which suffer from considerable biases (Wilhelm et al., 2017). As such, meteor radars are well-suited to study interannual tidal variability.

Tides have been observed to vary on scales from days (D. V. Pancheva et al., 2006) to years (Lieberman et al., 2007) and this variability has been proposed due to many mechanisms. On short timescales, these include: variability in the tropospheric source (Vial et al., 1994; Lieberman et al., 2007), changes in the mean flow that impact tidal propagation into the MLT (Ekanayake et al., 1997), interaction with planetary waves (Teitelbaum & Vial, 1991; D. V. Pancheva et al., 2006), and interaction with gravity waves (McLandress & Ward, 1994).

On long timescales, interannual variations in the MLT tidal amplitudes have been linked to changes in:

- solar variability (e.g. Namboothiri et al. (1993); Bremer et al. (1997); C. Beldon et al. (2006); Guharay et al. (2019)),
- the El Niño Southern Oscillation (ENSO) (e.g., Lieberman et al. (2007); Pedatella and Liu (2012); H. Liu et al. (2017); Sundararajan (2020) amongst others),
- Sudden Stratospheric Warmings (SSW) (e.g., Pedatella et al. (2021); G. Liu et al. (2021); R. E. Hibbins et al. (2019)),
- and the stratospheric Quasi-Biennial Oscillation (QBO) (e.g., R. Hibbins et al. (2007); Forbes et al. (2008); D. Pancheva et al. (2009); R. Hibbins et al. (2010); Laskar et al. (2016)).

We are also considering the Southern Annular Mode (SAM), and we also exclude SSWs from our analysis as we are focusing on indices with interannual variability rather than short-term or abrupt events. We will now discuss the mechanisms that could impact the tides for each of the indices mentioned earlier.

2 Mechanisms of Tidal Variability

The first mechanism we will discuss is solar flux. As tides are excited by the solar heating of ozone and water vapour in the stratosphere, changes in solar flux may cause variability in the tides. Sprenger and Schminder (1969) used observations from the mid-latitude to explore the effect of the solar cycle on the mesopause region wind and tides. They found a substantial positive correlation between solar radio flux and zonal/meridional prevailing winds during the winter and a negative link between solar flux and 12-hour tidal amplitude. This agrees with Greisiger et al. (1987) and Bremer et al. (1997), who found a negative correlation between solar flux and the 12-hour tidal amplitudes. Conversely, Guharay et al. (2019) investigated the long-term fluctuation of the tides in the MLT and their solar dependence using meteor radar. However, they identified that the tides have no substantial association with solar activity, agreeing with Jacobi et al. (1997).

Baumgaertner et al. (2005) also found a relationship between solar flux and tidal amplitudes measured by a medium frequency (MF) radar at Scott Base (78°S, 167°E), Antarctica. They found a negative correlation between solar activity and tidal amplitudes. They attribute the positive trends in tidal amplitudes to a rise in CO2 levels in the atmosphere. They propose that the cooling of the atmosphere produced by a rise in CO_2 might result in pressure and density drops. These reductions would increase tidal amplitudes associated with upward propagation.

Secondly, ENSO causes large-scale changes in tropospheric convection (K. E. Trenberth, 2002; Lieberman et al., 2007). These changes modify the tidal forcing in the troposphere, resulting in significant tidal variability in the MLT. Lieberman et al. (2007) performed modelling that revealed changes in tropospheric tidal heating during the 1997/1998 El Niño event responsible for observed changes in the 24-hour tidal amplitude in the MLT. Zonal mean winds in the stratosphere and mesosphere are also influenced by ENSO (Sassi, 2004). Changes in zonal mean zonal winds, in addition to changes in tropospheric tidal forcing, may have an impact on tides in the MLT by modifying tide vertical propagation (Pedatella & Liu, 2012).

Thirdly, QBO signatures have been found in both the 24- and 12-hour MLT tides. Forbes et al. (2008) found QBO modulations of ± 10 - 15% in 24-hour and 12-hour tidal amplitudes. They proposed that this was due to modulation by the QBO as the tides propagate from their tropospheric and stratospheric source regions into the MLT.

R. Hibbins et al. (2007, 2010) used the SuperDARN radar located at Halley, Antarctica (76°S, 27°W) and observed large QBO modulation of the summertime 12-hour non-migrating tide. Also, D. Pancheva et al. (2009) investigated temperature tides using data from Sounding of the Atmosphere using Broadband Emission Radiometry (SABER) and winds from the TIMED Doppler Interferometer (TIDI) onboard the Thermosphere Ionosphere Mesosphere Energetics and Dynamics (TIMED) satellite and saw QBO modulation of the migrating 12-hour tide at mid-latitudes in both hemispheres. Using a similar method, Xu et al. (2009) showed that the largest QBO modulations of the 24-hour tide in the MLT are in temperature at the equatorial region. However, the most considerable QBO modulation for winds was at 20°N and 20°S. de Araújo et al. (2017) also found that the strongest effect on the 24-hour tide by the QBO is seen during the equinoxes and early winter observed using a meteor radar over Cachoeira Paulista (22.7°S, 45.0°W), Brazil. Laskar et al. (2016) found that variations in the enhancement duration of the average 12-hour amplitudes during August-September are linked to low-latitude QBO winds by analysing meteor radar winds at 54°N and 69°N with Modern Era-Retrospective Analysis for Research and Applications (MERRA) zonal winds.

Fourth, the SAM describes the north/south movement of the belt of eastward winds centred at 50/55° latitude (Marshall, 2003). It substantially impacts the climatic systems of the southern hemisphere's high and mid-latitudes and influences climate variability and change in the southern hemisphere. The surface zonal winds of SAM and the southern hemisphere greatly impact the atmospheric and oceanic circulation systems (Lee et al., 2019; Abram et al., 2014). Hence we may see evidence of this at greater heights, such as in the MLT. For example, Merzlyakov et al. (2009) found no significant link between SAM and the MLT. They investigated wind measurements from a meteor radar situated at Molodezhnaya (67.7°S, 45.9°E) and MF radars at Mawson (67.6°S, 62.9°E) and Davis (68.6°S, 78.0°E).

In Section 3, we describe the radar, data and the climate indices we have used. Section 4, describes the methods used to obtain monthly tidal amplitudes from hourly winds and, secondly, the linear regression used to extract the time-series contribution to the tidal amplitudes from the climate indices. In Section 6, we consider our results compared to other studies and suggest possible mechanisms linking tidal amplitudes in the MLT and climate indices. Finally, in Section 7, we present a summary of our findings.

3 Data

3.1 Meteor Radar

We have used tidal amplitudes obtained from hourly winds measured in the MLT by a SKiYMET VHF meteor radar located at Rothera (68°S, 68°W) from 1st January 2005 to 31st December 2020. Meteor radar is a well-established method of measuring MLT winds from 75 to 105 km (e.g. Stober, Kuchar, et al. (2021); Dempsey et al. (2021); Davis et al. (2013); C. Beldon et al. (2006); Mitchell (2002)) and provides us with a robust set of measurements to perform our linear regression. This radar was installed in 2005 and has operated for most of the period from 2005 to 2020. Note that there are instances in the dataset where data has been removed due to quality issues. During these periods, the meteor height distribution exhibited a large increase in spread, meaning data from this period is not trustworthy (see grey areas in Figure 2).

The Rothera radar employs a solid-state transmitter with a peak power of 6 kW. In 2019, the antennae were replaced following weather-related degradation. This reduced the fraction of ambiguous meteors detected. The radar antenna receiver array uses five interferometer elements to measure echo azimuth and zenith angles. When combined with range data, this allows the height of individual meteor echoes to be determined. A detailed description of the SKiYMET radar operation is given by Hocking et al. (2001).

3.2 Time Series of Indices

To qualify the dependence of tidal amplitudes on specific climate indices, we regress monthly values of five climate indices and time against 12-hour tidal amplitudes. These indices are F10.7 solar flux, ENSO, QBO10, QBO30 and SAM.

Observed solar flux F10.7 index is the solar radio flux at 10.7 cm radio emission measured on the surface of Earth. It is one of the longest-running records of solar activity, and so we can use it as an indicator of solar activity in our linear regression. It is measured in solar flux units (SFU), with 1 SFU equal to 10^{-22} W m^{-2} Hz^{-1}.

For the El Niño Southern Oscillation, we use the Niño 3.4 index, representing the average equatorial sea surface temperatures (SST) in a box bound by 5°N - 5°S, 170°W - 120°W. This index uses a 5-month running mean, and the El Niño or La Niña events are defined when the Niño 3.4 SSTs exceed +/- 0.4C for six months or more (K. Trenberth, 2021).

For the Quasi Biennial Oscillation (QBO) indices, the zonal mean zonal wind (in ms^{-1}) is averaged over 5°N to 5°S at 10 hPa for the QBO10 index and at 30 hPa for the QBO30 index. For the Southern Annular mode, we use the Marshall Southern Annular Mode index (SAM index) which is the difference between the normalised monthly zonal sea level pressure (SLP) at 40°S minus the normalised monthly zonal sea level pressure at 65°S (Marshall, 2003).

Figure 1 presents the time series of the five climate indices over the 2005 to 2020 period. Our chosen period encompasses the entirety of solar cycle 24, which has a minimum in December 2008 and the following minimum in December 2019, shown in Figure 1a. In Figure 1b, the ENSO index varies systematically from 25 K to 29 K but with-

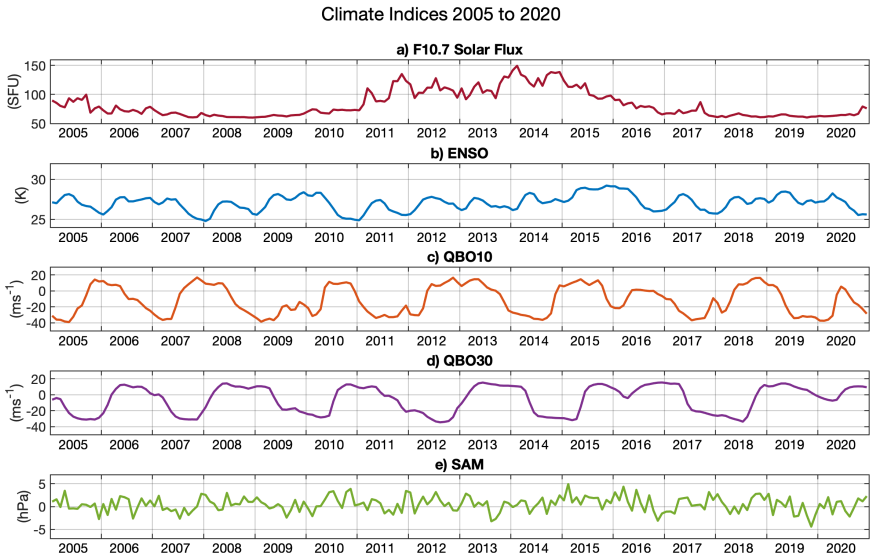

Figure 1: Time-series of the global climate indices of (a) F10.7 Solar Flux, (b) ENSO, (c) QBO10, (d) QBO30 and (e) SAM for the period 2005 to 2020.

out a strongly-fixed period. The QBO10 index in Figure 1c has a more defined period, with a regular period of around 22 months. This is similar to the QBO30 (in Figure 1d) index which has a similar period but lagged by around 9 months from the QBO10 index. Finally, in Figure 1e, the SAM index does not have a strong periodicity with no apparent trend.

4 Method

4.1 Tidal Amplitudes from Hourly Winds

To investigate the interannual variability of the tides in the mesosphere and lower thermosphere, we calculate amplitudes of the 12-hour tide using meteor radar hourly winds. Hourly winds are estimated using the radial velocity measurements taken from each individual meteor, assuming that the flow is horizontal and uniform across the meteor collecting volume at any given height. We calculate the winds by combining the inferred horizontal velocities obtained for each meteor with a Gaussian weighting in height and time around a specific height and specific time. The full-width-half-maxima for these Gaussian weightings are 2 h in time and 3 km in height. The centre of the Gaussian progresses across the data in 1 hour time and 1 km height steps, giving hourly winds between 79 - 101 km. We obtain tidal amplitudes by creating a monthly composite day of the winds and fitting sinusoidal waves of tidal periods to the composite day. These have periods of 24, 12, 8 and 6 hours. For more detail on the Gaussian weighting method, see Hindley et al. (2021), and for more information on the tide fitting, see Dempsey et al. (2021). We will be using only the 12-hour tide for this study as this tide has the largest amplitude at this latitude.

4.2 Linear Regression

To investigate how the climate indices interact with the amplitude of the 12-hour tide, we use a linear regression analysis, allowing us to investigate possible explanations for the interannual variability of tidal amplitudes in the MLT. We apply this to the tidal amplitude anomaly (e.g., the January 2020 anomaly is defined as the January 2020 monthly mean tidal amplitude minus the climatological monthly mean tidal amplitude for January), similarly to Gan et al. (2017) and Ramesh et al. (2020). This step ensures that we have removed the seasonal cycle.

We split up our data into three month windows as the climate indices' response my differ in each season. Therefore, multiple models are used to create a year. We then repeat this for each height from 79 to 101 km. We run the models on the zonal and meridional components separately to create output for each component.

We use the following expression for the linear model:

$$A'_{12} = \beta_0 + (\beta_1 F10.7) + (\beta_2 ENSO) + (\beta_3 QBO10) + (\beta_4 QBO30) + (\beta_5 SAM) + (\beta_6 Time) \quad (1)$$

where A'_{12} is the 12-hour tidal amplitude minus the seasonality, β_0 is the constant and β_1 to β_6 are the coefficients of the climate variables.

A linear regression method allows us to decompose the interannual variability in the tidal amplitude into possible causes, such as the climate variables we are considering. However, we should note that there are other causes of variability in the atmosphere other than any trends in the MLT or the five variables we use in this study. Further, the atmosphere is not a wholly linear system. For example, interactions exist between tides and planetary waves, which are non-linear. Therefore, the results that we produce are a simplification of interactions in the atmosphere. Despite this, the linear regression methodology allows us to investigate any linear correlations between tidal amplitudes in the MLT and climate variables.

4.2.1 Multicollinearity

For the linear regression to be valid, we need to check for multicollinearity, that is, that none of the indices used are correlated with each other. If that were the case, then the results from our linear regression would be unreliable. This test ensures solar flux, ENSO, QBO10, QBO30, SAM, and time are independent of each other. The test to determine this is to calculate Variance Inflation Factors (VIFs).

VIFs are created by firstly regressing each independent variable against the others and then calculating the VIF as follows:

$$VIF = \frac{1}{(1 - R^2)} \quad (2)$$

where R^2 is the R-squared value. The values of the VIF range from 1 to infinity, with values around 1 suggesting that there is no multicollinearity; values between 1 and 5 suggesting some multicollinearity, but not enough to disrupt the model; values over 5 suggesting correlation and are cause for concern; and values over 10 are a major problem and imply a strong correlation (Kalnins, 2018). For our linear regression, the VIFs range from 1.02 to 1.35. As our values are around 1, the variables we have chosen to explain tidal amplitude variability do not suffer from multicollinearity, and therefore, we can use them confidently.

4.2.2 Auto-correlation

To perform a linear regression, we assume that the residuals are free from auto-correlation, which means the residuals from the linear regression are not correlated with each other.

Auto-correlation would indicate that essential information is missing from the model and that we cannot rely on the standard errors.

To determine the presence of auto-correlation, we use the Durbin-Watson (DW) test which yields a number between 0 and 4. A score of 2 indicates no auto-correlation, whereas results closer to 0 indicate positive auto-correlation, and results closer to 4 indicate negative auto-correlation. It follows that readings between 1.5 and 2.5 are normal and results below 1 and above 3 indicate some form of auto-correlation (Webster, 2012).

Because we create many models to describe the tidal amplitudes, we have many DW statistics. The meteor radar tidal amplitude DW statistics all lie in the acceptable 1 to 3 range, with 86% falling in the 1.5 to 2.5 range. Therefore, our DW results all fall within the acceptable range. So, while there will be some small uncertainty about the standard errors for a subset of models, the vast majority of models are not affected.

5 Results

5.1 12-hour Tidal Amplitudes

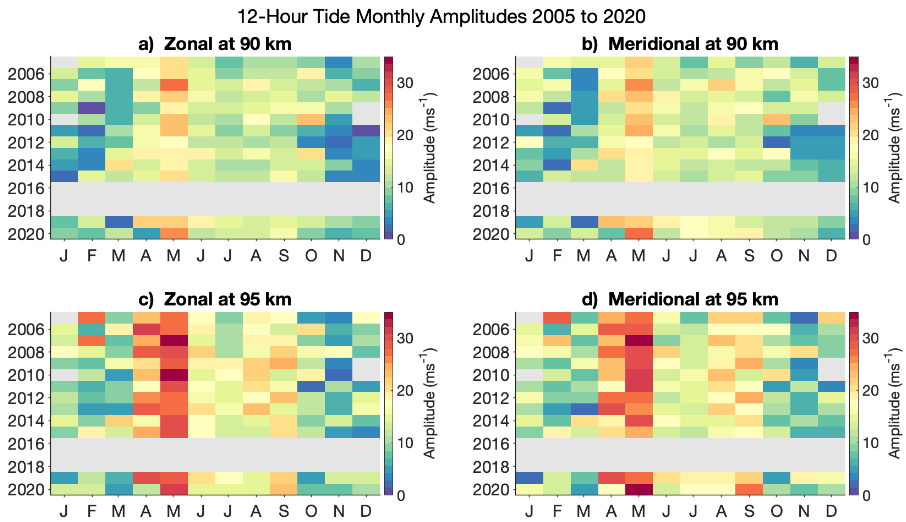

Figure 2: Monthly 12-hour tidal amplitudes for the period 2005 to 2020 for (a) zonal at 90 km, (b) meridional at 90 km, (c) zonal at 95 km and (d) meridional at 95 km. Each coloured box represents the monthly tidal amplitude. The grey bars indicate where data has been removed due to quality issues.

Figure 2 presents the zonal and meridional tidal amplitudes at 90 km and 95 km from 2005 to 2020. We can see in each panel that there is considerable interannual variability. Each month exhibits a range of amplitudes over 2005 to 2020. For example, the month of May typically has the largest amplitudes and exhibits a substantial variability in measured amplitude across the years. In Figure 2a, we can see May 2007 exhibits values of around 27 ms^{-1}, whereas in 2012, the month of May exhibits amplitudes of 15 ms^{-1}. In Figures 2a and b, we can see that in December (during austral summer) at 90 km, there is a large decrease in amplitudes from 2011 to 2015. At 95 km, in Figures 2c and d, this is not repeated. We again see that May has the largest amplitudes at this height, reaching 35 ms^{-1}. In each panel, every month exhibits considerable variability between years, and therefore, there is enough evidence to proceed with our investigation.

5.1.1 Average Year 12-hour Tide

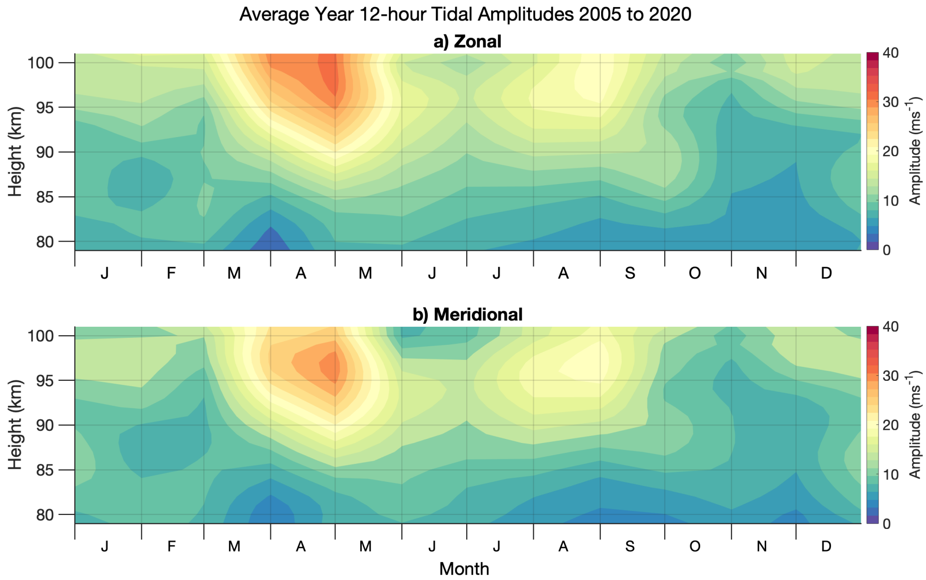

Figure 3: Average year 12-hour tidal amplitudes over the height range 80 to 100 km for the period 2005 to 2020 for (a) zonal and (b) meridional components.

Once we have calculated the tidal amplitudes, we calculate an average year for our data set, shown in Figure 3. Figure 3a presents the average year zonal tidal amplitudes. We can see that there are two peaks in amplitude across the year, representing the semi-annual cycle in tidal amplitudes peaking close to the equinoxes. In April, the first peak reaches amplitudes $\sim$ 40 ms^{-1} above 95 km, sustaining until mid-May. The second peak occurs in August but with a smaller amplitude of around 24 ms^{-1}. The smallest tidal amplitudes are found near 80 km towards the end of March and early April, where tidal amplitudes are near 0 ms^{-1}. In general, larger amplitudes exist between March and September above 90 km, whereas smaller values exist between October and February especially near 80 km.

Figure 3b presents the average year meridional tidal amplitudes. Similarly to Figure 3a, the tidal amplitudes display a semi-annual cycle with two peaks in amplitude in April and late August. Compared to the zonal, these peaks occur at a similar height and again close to the equinoxes.

5.1.2 Tidal Anomaly

We have seen considerable interannual variability in the tidal amplitudes in Figure 2 and the average seasonal cycle of tidal amplitudes in Figure 3. To extract the variability within the dataset without the semi-annual cycle, we subtract the average year from each year of the dataset, leaving the amplitude anomaly presented in Figure 4.

From both Figures 4a and b, we see that the dataset exhibits large variability. The most considerable differences are often seen at the upper heights, especially in Figure

4a from 2006 to 2009, where the large repeated dark red stripes indicate increases relative to the average year. The meridional component in Figure 4b exhibits more negative deviations from the average than the zonal component. This is especially clear from 2011 to 2013.

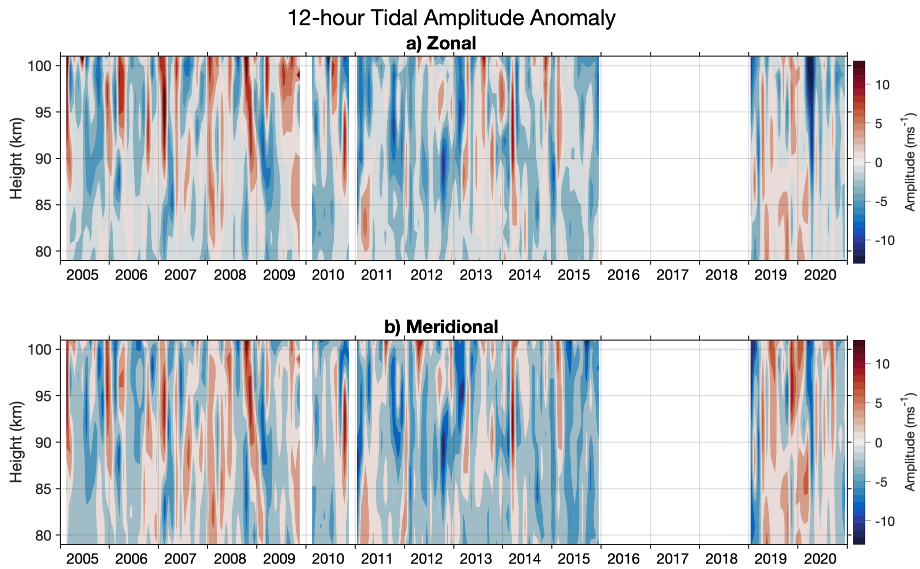

Figure 4: 12-hour tidal amplitude anomaly over the height range 80 to 100 km for the period 2005 to 2020 for the (a) zonal and (b) meridional components. The white areas represent data removed for quality reasons. Red and blue colours represent positive and negative amplitude anomalies, respectively.

5.2 Correlation of Climate Variables to Interannual Tidal Variability

Next, we explore the output from our linear regression analysis on the tidal amplitudes from the meteor radar. We present time-height contours of the coefficients from the linear regression for each climate index. For each, we have overlaid contours representing the significance level using t-test statistics (from a two-tailed student's t-test), with the dashed contour representing the 80% confidence level and the solid contour indicating the 90% significance level. In all of the indices used in this study, we use contribution to suggest a link between the index being studied and the variability of the 12-hour tidal amplitude in the MLT. We do not intend to imply that any such correlations imply causation.

For each index, we have scaled the colour bar axis using the interdecile range, the difference between the 90th and 10th percentile of the index. This is represented by α in each plot and Table 1 presents these values for each index. As the indices are not separated into zonal and meridional components, the α value is the same for the contributions' zonal and meridional components.

5.2.1 Solar Flux

F10.7 solar flux results are presented in Figure 5. The most noticeable feature in both the zonal (Figure 5a) and the meridional (Figure 5b) is the large negative contribution at the beginning of the year and at the end of the year, between 85 and 93 km.

Index	α
F10.7 Solar Flux	57.6 SFU
ENSO	2.67 K
QBO10	45.8 ms^{-1}
QBO30	42.8 ms^{-1}
SAM	4.02 hPa

Table 1: The scaling value, α, used to scale the linear regression contribution plots (Figures 5 to 10) for each given index.

We see a contribution of up to -4 ms^{-1} per α SFU solar flux ($\alpha = 57.6$ SFU). The meridional component also has a large statistically-significant region in mid-June, extending through December and into February. In the middle of the year, this contribution is -3 ms^{-1} per α SFU in June at 90 km, growing to -4 ms^{-1} per α SFU at 90 km in December.

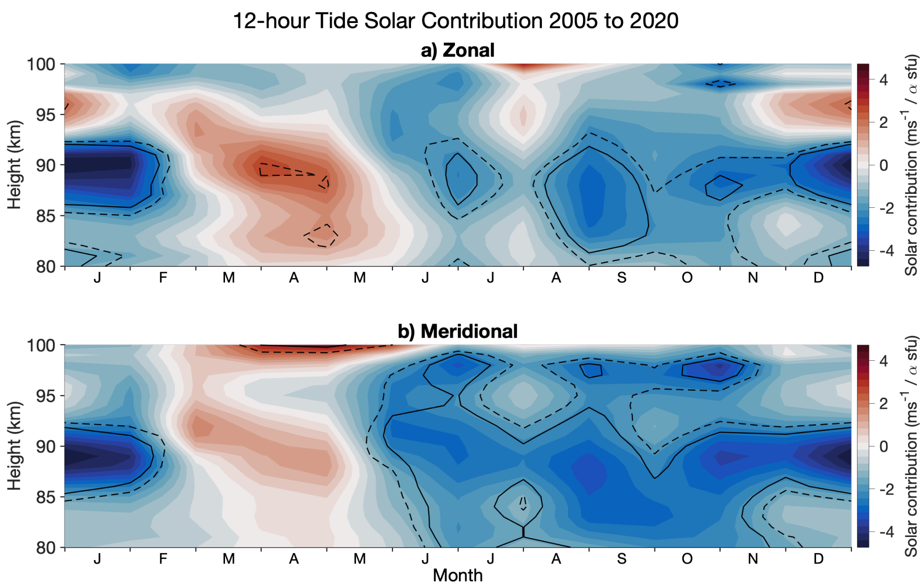

Figure 5: 12-hour tide F10.7 Solar Flux contribution to tidal amplitudes over the height range 80 to 100 km for the period 2005 to 2020, for the (a) zonal and (b) meridional components. Dashed and solid contours indicate the 80% and 90% confidence intervals, respectively, according to the t-test.

5.2.2 ENSO

The results for El Niño Southern Oscillation (ENSO) are presented in Figure 6. ENSO does not present much significance compared to the other indices used in this study. The only notable feature in both components is a small significant region below 82 km in height from late February to April with a contribution of -3 ms^{-1} per α K, where $\alpha = 2.67$ K.

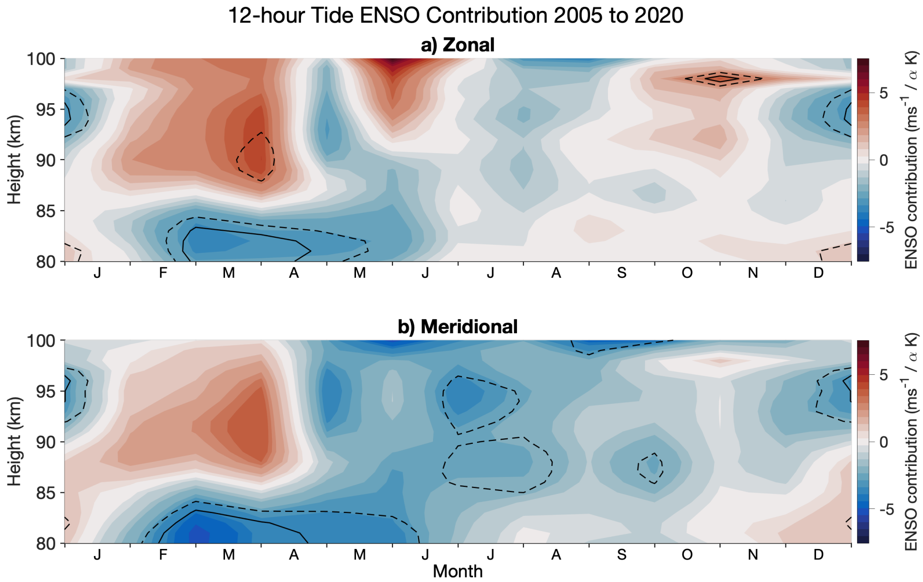

Figure 6: 12-hour tide ENSO contribution to tidal amplitudes over the height range 80 to 100 km for the period 2005 to 2020, for the (a) zonal and (b) meridional components. Dashed and solid contours indicate the 80% and 90% confidence intervals, respectively, according to the t-test.

5.2.3 QBO at 10 hPa

The QBO10 index is presented in Figures 7a and b for the zonal and meridional components, respectively. The most striking feature in this Figure is a strong negative contribution of -5 ms^{-1} per α ms^{-1} QBO10 from December to January at most heights (where $\alpha = 45.8$ ms^{-1} QBO10). This feature is also found in the zonal component but is weaker.

Both components also have significant regions in the middle of the year. In the zonal component, this is seen from May to June centred at 95 km with a 4 ms^{-1} per α ms^{-1} QBO10 and in the meridional, we see a -3 ms^{-1} per α ms^{-1} QBO10 contribution from June to July centred on 95 km.

5.2.4 QBO at 30 hPa

The QBO30 index in the meridional, Figure 8b, exhibits a strong negative contribution in January of -6 ms^{-1} per α ms^{-1} QBO30 above 95 km and -4 ms^{-1} per α ms^{-1} QBO30 below 90 km during January (where $\alpha = 42.8$ ms $^{-1}$). Unlike QBO10, this feature is not reflected in the zonal component in Figure 8a.

5.2.5 SAM

The SAM results are presented in Figure 9. In both the zonal and meridional components, Figure 9a and b, respectively, there are significant regions from December to January above 90 km. This reaches -5 ms^{-1} per α hPa SAM (where $\alpha = 4.02$ hPa).

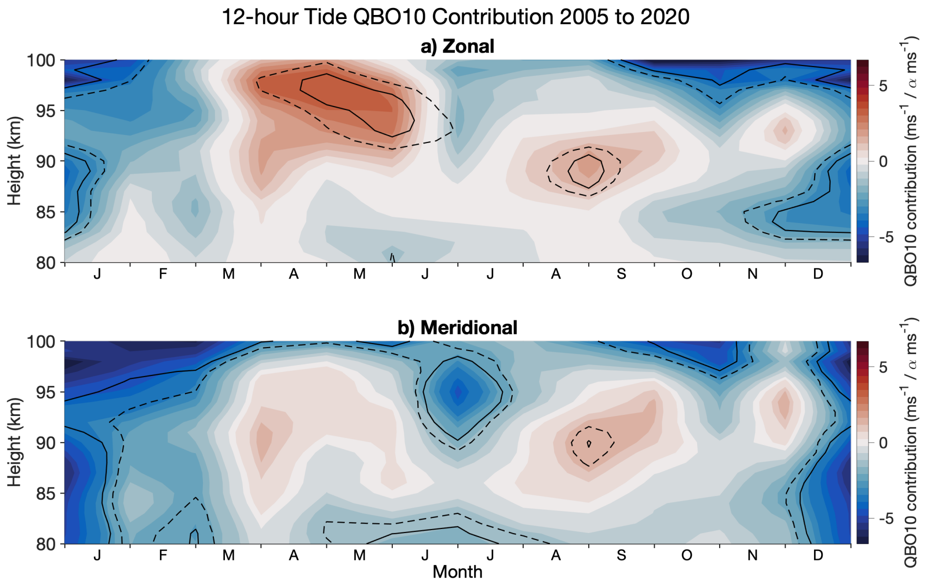

Figure 7: 12-hour tide QBO10 contribution to tidal amplitudes over the height range 80 to 100 km for the period 2005 to 2020, for the (a) zonal and (b) meridional components. Dashed and solid contours indicate the 80% and 90% confidence intervals, respectively, according to the t-test.

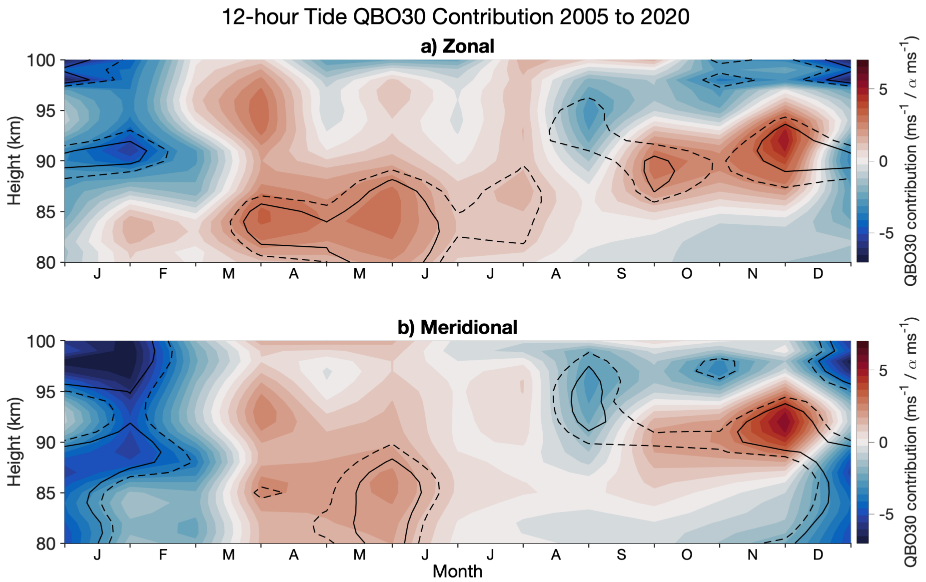

Figure 8: 12-hour tide QBO30 contribution to tidal amplitudes over the height range 80 to 100 km for the period 2005 to 2020, for the (a) zonal and (b) meridional components. Dashed and solid contours indicate the 80% and 90% confidence intervals, respectively, according to the t-test.

We also see a positive contribution in each component in February to April above 95 km. Here we see contributions of 5 ms^{-1} per α hPa.

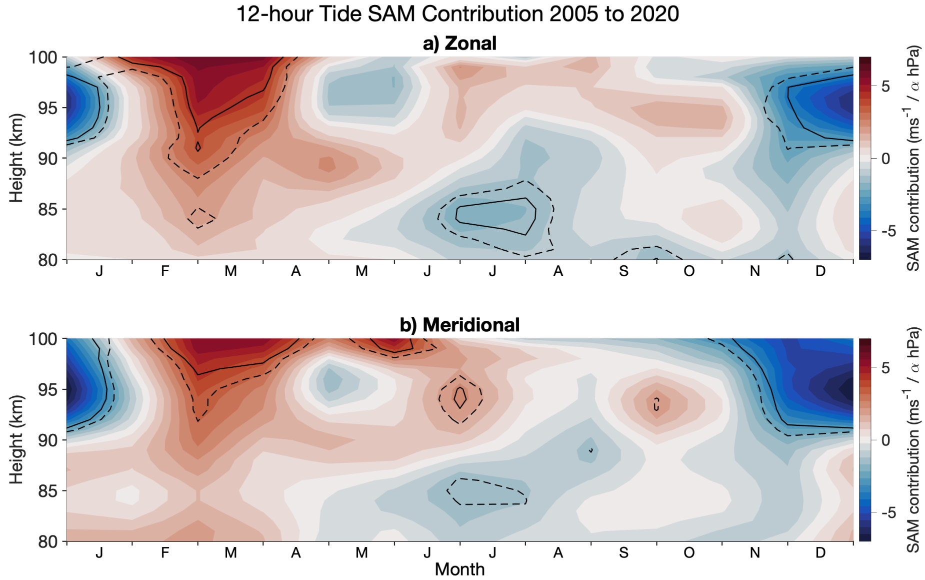

Figure 9: 12-hour tide SAM contribution to tidal amplitudes over the height range 80 to 100 km for the period 2005 to 2020, for the (a) zonal and (b) meridional components. Dashed and solid contours indicate the 80% and 90% confidence intervals, respectively, according to the t-test.

5.2.6 Time

The results for time, or the presence of linear trends, are presented in Figure 10. A large significant region from February to June above 90 km in the zonal component, Figure 10a, indicates a -1 ms^{-1}/year contribution. However, in the meridional component, Figure 10b, all significant regions correspond to minimal contributions. For example, in late August, above 87 km, there is a contribution of 0.2 ms^{-1}/year, which is very small compared to monthly tidal amplitudes in the same month, which can be as large as 25 ms^{-1}.

6 Discussion and Conclusions

6.1 Interannual variability

We have investigated the possible relation between the 12-hour tide in the Antarctic MLT using meteor radar measurements and the climate indices solar flux, ENSO, QBO10, QBO30, SAM and time by performing a linear regression on the 12-hour tidal amplitudes for the period between 2005 and 2020 inclusive. We have found that solar flux, QBO10, QBO30, SAM, and time all have varying degrees of correlation with the amplitudes of the zonal and meridional 12-hour tide. In contrast, we have found minimal correlation between ENSO and the 12-hour tidal amplitudes.

In Figure 2, we presented the 12-hour monthly mean tidal amplitudes at 90 and 95 km as measured at Rothera (68°S, 68°W). We reported a seasonal cycle, also seen by Stober, Janches, et al. (2021) and C. L. Beldon and Mitchell (2010). We found that

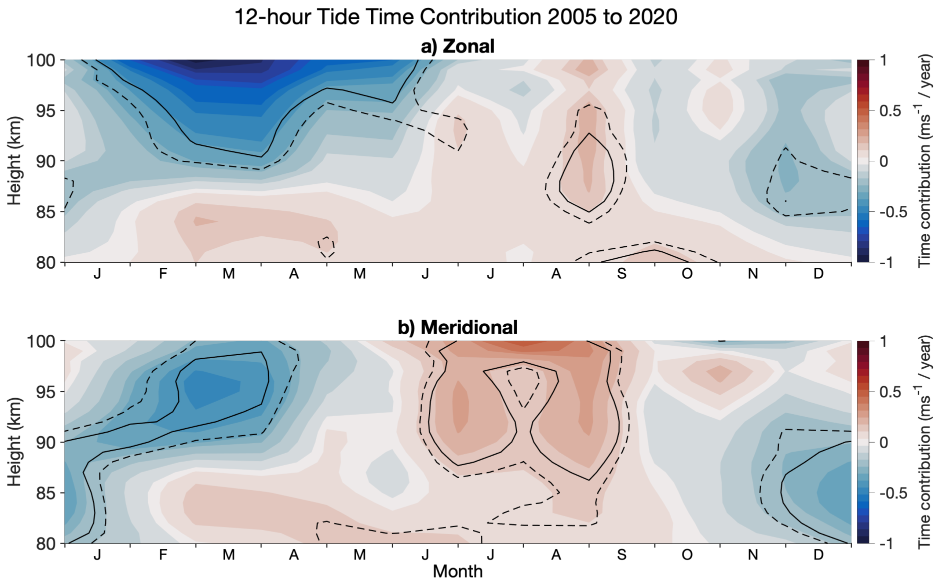

Figure 10: 12-hour tide time contribution to tidal amplitudes over the height range 80 to 100 km for the period 2005 to 2020, for the (a) zonal and (b) meridional components. Dashed and solid contours indicate the 80% and 90% confidence intervals, respectively, according to the t-test.

there is considerable interannual variability in the tidal amplitudes in the MLT, consistent with Baumgaertner et al. (2005) and Merzlyakov et al. (2009). Further, Conte et al. (2017) measured the amplitude of the 12-hour tide at Davis (69°S, 78°E) using a meteor radar and found some interannual fluctuation. They identified less variability in the 12-hour tide in winter, with summer showing more variability. Baumgaertner et al. (2005) found that the seasonal behaviour of the 12-hour tide bears a striking resemblance to the behaviour of planetary wave activity at high latitudes. They hypothesised that planetary waves contribute not only to the seasonal behaviour but also the interannual variation of the tide.

6.2 Context with other instruments

The meteor radar we used is located at the British Antarctic Survey's Rothera base, which also has an MF radar used to measure tides in the MLT. R. Hibbins et al. (2007) used data collected between 1997 and 2005 to calculate tidal amplitudes and phases. They reported a 12-hour tide with a semi-annual cycle peaking in April and September, as we observed using the meteor radar at Rothera, and a 24-hour tide peaking in January and February with amplitudes of roughly 8 ms^{-1}.

The tidal amplitudes we observed in Figure 2 at 95 km are larger than those observed at 90 km. The amplitude growth with height is an obvious disagreement between R. Hibbins et al. (2007) and the meteor radar results. Our data shows considerable amplitude increases over 5 km, contrasting with the MF observations, which showed consistent amplitudes throughout all heights. The disparity between R. Hibbins et al. (2007) and our findings could be explained by a known bias between MF and meteor radar in the MLT, where MF radars are found to under-represent ambient winds, especially above 80 km (Manson et al., 2004; Hines et al., 1993).

The disparities, according to Wilhelm et al. (2017), are due to two factors. To begin with, the observed centre of scatter of the MF beam is not always the same as the centre of the beam volume, which weights the measurement to a lower zenith angle and hence a greater height in most circumstances. This is important above 92 km due to the spreading of the beam. Second, the scattering mechanism itself causes considerable variations between the main lobe of a vertical pointed, narrow Doppler beam and the appropriate side lobes, making radial velocity measurements over 92 km inaccurate. As a result, MF radars are more adapted to detecting the atmosphere at heights less than 80 km, and MLT tidal analysis is better suited to meteor radar capabilities.

6.3 Correlations between tidal amplitudes and climate indices

We used linear regression to investigate possible links in changes in tidal amplitudes to changes in the climate indices. We have found that solar flux, QBO, SAM and time all have correlations, whereas ENSO does not show an extensive significant correlation.

6.3.1 Solar Cycle

We found correlations at the 90% significance level during summer suggesting a -4 ms^{-1} per α SFU ($\alpha = 57.6$ SFU) in both the zonal and meridional components at 85 to 93 km in height from December to mid-February. This significant region begins in mid-June in the meridional but becomes strong in December. This implies a negative correlation between F10.7 and the 12-hour tide amplitude.

Similarly, at Saskatoon (52°N, 107°W), Namboothiri et al. (1993) found a negative correlation between the solar cycle and tides at the solstices and Bremer et al. (1997) found a weak negative correlation between solar activity and the zonal 12-hour tide during most months of the year using a range of mid and high-latitude northern hemisphere stations. C. Beldon et al. (2006) investigated the 8-hour tide in the MLT over the UK from 1988 to 2004. They found interannual variability in the amplitude of the 8-hour tide and a possible role of solar variability influencing the behaviour of the tide and a trend between summer mean amplitudes and F10.7. As the 8-hour tide has been hypothesised to be excited in part by non-linear interactions between the 12- and 24-hour tides, this provides further evidence of solar flux influencing tidal amplitudes in the MLT.

Conversely, Guharay et al. (2019) used meteor radar to investigate long-term variability of the tides in the MLT and their solar dependence at a low-latitude station at Cachoeira Paulista (22.7°S, 45°W). They found that the tides do not show any significant relationship with solar activity, in agreement with Jacobi et al. (1997) measured from Collm Observatory of the University of Leipzig (52°N, 15°E).

An explanation for the reduction we see in tidal amplitudes following an increase in solar flux may be explained through the different excitation mechanisms of migrating and non-migrating modes. The non-migrating modes are created by non-linear interactions between the migrating modes and planetary waves. However, the migrating modes are sun following and excited via solar flux. We observe a superposition of these two modes with the meteor radar. Therefore, an increase in the migrating mode may also increase the non-migrating mode as more interactions can occur. These may be excited in an opposite phase to the migrating mode and could effectively cancel out the migrating mode; consequently, we observe a smaller tidal amplitude.

6.3.2 ENSO

In the present study, we have found a small instance of significance between the ENSO index and monthly 12-hour tidal amplitudes. Further, H. Liu et al. (2017) simulated that a ground-based station located south of the equator would detect a substantial enhancement of the 24-hour tide in the meridional component during both El Niño and La Niña but only during El Niño in the zonal component and temperature. Our region of significance coincided with a small contribution. Therefore, we can conclude that ENSO shows no extensive significant correlation with monthly tidal amplitudes.

6.3.3 QBO

For both the QBO10 and QBO30 indices, we have seen significant correlations. These have been more prominent in the meridional component in the summertime, where we have seen correlations of -5 ms^{-1} per α ms^{-1} QBO10. (Mayr, 2005) used the Numerical Spectral Model (NSM) and found QBO modulations of the tide. They found that above 80 km, the QBO related interannual variations of the tide are relatively large and generated primarily by gravity wave momentum deposition. Therefore, the magnitude of the tide's QBO modulation in the upper mesosphere varies considerably. They attribute the intermittency of the QBO modulation of the tide to non-linear interactions and gravity wave drag.

Moreover, Laskar et al. (2016) found that QBO wind modulates the northern mid-latitude and high-latitude 12-hour tide during the August–September period. They proposed that the QBO modulation process consists of two steps: firstly, during August–September, the northern hemispheric 12-hour tides have increased amplitudes, which may be due to in-phase interaction between SW2 and SW1 (12-hour, semi-diurnal, westward propagating wave numbers 1 and 2, respectively). Secondly, the ducted quasi-stationary planetary waves of wavenumber 1 from the southern hemisphere interacts with the northern hemispheric mid-latitude and high-latitude 12-hour tides (particularly SW1) to imprint its signature on the 12-hour tides. Therefore, the enhancements that we observe may be due to this mechanism.

6.3.4 SAM

We have found that above heights of 90 km, there is a significant correlation from mid-February to mid-April with a positive contribution of 5 ms^{-1} per α hPa (where $\alpha =$ 4.02 hPa). There is then a period of negative contribution from mid-November to mid-January with a -5 ms^{-1} per α hPa. A potential reason for the correlation coefficient for SAM growing above 90 km may be due to tidal amplitudes also growing across the height range we are considering. The SAM may have the same percentage contribution across the height range but only becomes significant at upper heights where the tide is large. Therefore, a larger amplitude tide may give a larger contribution. In contrast, Merzlyakov et al. (2009) sought to identify any correlations between the SAM index and MLT winds; however, they did not find any correlation.

7 Summary

This study has utilised a 15 year long data set of 12-hour tidal amplitudes from a meteor radar located at the British Antarctic Survey base at Rothera (68°S, 68°W). We have investigated the interannual variability of the tidal amplitudes using a linear regression analysis to identify any links between climate indices and the 12-hour tidal amplitudes in the zonal and meridional components.

We have found:

1. Persistent large-amplitude 12-hour tide throughout the period 2005 to 2020 at Rothera, which dominates the wind field of the MLT. The 12-hour tidal amplitudes show large interannual variability. For example, the interdecile range at 95 km in height of the monthly mean tidal amplitudes in spring of 17.2 ms^{-1}, 12.6 ms^{-1} in summer, 23.6 ms^{-1} in autumn and 9.0 ms^{-1} in winter.

2. The climatological tides we observed are larger than those observed using MF radars at similar latitudes due to MF radar bias at 80 to 100 km in height.
3. Using a linear regression analysis to break down this interannual variability, we have discovered that F10.7, QBO10, QBO30 and SAM all have significant correlations with the 12-hour tidal amplitudes.

This work suggests that climate phenomena in the troposphere and stratosphere may influence the tides in the MLT. This implies that the atmospheric tides are an important coupling mechanism between the lower and upper atmosphere.

Data Availability

The meteor radar data used in this study is from Mitchell, N. (2019): University of Bath: Rothera Skiymet Meteor Radar data (2005 – present). Centre for Environmental Data Analysis, 2022. `https://catalogue.ceda.ac.uk/uuid/aa44e02718fd4ba49cefe36d884c6e50`. The 10.7cm Solar Flux Data are provided as a service by the National Research Council of Canada.

Acknowledgments
SMD and PEN are supported by a NERC GW4+ Doctoral Training Partnership studentship from the Natural Environment Research Council (grant nos. for SMD: NE/L002434/1 and PEN: NE/S007504/1) and is thankful for the support and additional training provided. TMG, CJW and NJM are supported by the UK Natural Environment Research Council (grant nos. NE/R001391/1 and NE/R001235/1).

CRediT authorship contribution statement

Shaun M. Dempsey: Writing - Original draft preparation, Methodology, Software, Lead Formal Analysis, Investigation, Data Curation. Phoebe E. Noble: Writing - Review, Software, Formal Analysis, Investigation, Data Curation, Validation. Tracy Moffat-Griffin: Supervision, Writing - Review and Editing, Validation, Resources. Corwin J. Wright: Supervision, Validation, Writing - Review, Resources. Nicholas J. Mitchell: Supervision, Methodology, Conceptualisation, Resources.

References

Abram, N. J., Mulvaney, R., Vimeux, F., Phipps, S. J., Turner, J., & England, M. H. (2014, May). Evolution of the southern annular mode during the past millennium. *Nature Climate Change*, *4*(7), 564–569. Retrieved from `https://doi.org/10.1038/nclimate2235` doi: 10.1038/nclimate2235

Baumgaertner, A., McDonald, A., Fraser, G., & Plank, G. (2005, November). Long-term observations of mean winds and tides in the upper mesosphere and lower thermosphere above scott base, antarctica. *Journal of Atmospheric and Solar-Terrestrial Physics*, *67*(16), 1480–1496. Retrieved from `https://doi.org/10.1016/j.jastp.2005.07.018` doi: 10.1016/j.jastp.2005.07.018

Beldon, C., Muller, H., & Mitchell, N. (2006, March). The 8-hour tide in the mesosphere and lower thermosphere over the UK, 1988–2004. *Journal of Atmospheric and Solar-Terrestrial Physics*, *68*(6), 655–668. Retrieved from `https://doi.org/10.1016/j.jastp.2005.10.004` doi: 10.1016/j.jastp.2005.10.004

Beldon, C. L., & Mitchell, N. J. (2010, September). Gravity wave–tidal interactions in the mesosphere and lower thermosphere over rothera, antarctica (68°s, 68°w). *Journal of Geophysical Research*, *115*(D18). Retrieved from `https://doi.org/10.1029/2009jd013617` doi: 10.1029/2009jd013617

Bremer, J., Schminder, R., Greisiger, K., Hoffmann, P., Kürschner, D., & Singer, W. (1997, March). Solar cycle dependence and long-term trends in the wind field of the mesosphere/lower thermosphere. *Journal of Atmospheric and Solar-Terrestrial Physics*, *59*(5), 497–509. Retrieved from `https://doi.org/10.1016/s1364-6826(96)00032-6` doi: 10.1016/s1364-6826(96)00032-6

Conte, J. F., Chau, J. L., Stober, G., Pedatella, N., Maute, A., Hoffmann, P., ... Murphy, D. J. (2017, July). Climatology of semidiurnal lunar and solar tides at middle and high latitudes: Interhemispheric comparison. *Journal of Geophysical Research: Space Physics*, *122*(7), 7750–7760. Retrieved from `https://doi.org/10.1002/2017ja024396` doi: 10.1002/2017ja024396

Davis, R. N., Du, J., Smith, A. K., Ward, W. E., & Mitchell, N. J. (2013, September). The diurnal and semidiurnal tides over ascension island (° s, 14° w) and their interaction with the stratospheric quasi-biennial oscillation: studies with meteor radar, eCMAM and WACCM. *Atmospheric Chemistry and Physics*, *13*(18), 9543–9564. Retrieved from `https://doi.org/10.5194/acp-13-9543-2013` doi: 10.5194/acp-13-9543-2013

de Araújo, L. R., Lima, L. M., Jacobi, C., & Batista, P. P. (2017, March). Quasi-biennial oscillation signatures in the diurnal tidal winds over cachoeira paulista, brazil. *Journal of Atmospheric and Solar-Terrestrial Physics*, *155*, 71–78. Retrieved from `https://doi.org/10.1016/j.jastp.2017.02.001` doi: 10.1016/j.jastp.2017.02.001

Dempsey, S. M., Hindley, N. P., Moffat-Griffin, T., Wright, C. J., Smith, A. K., Du, J., & Mitchell, N. J. (2021, January). Winds and tides of the antarctic mesosphere and lower thermosphere: One year of meteor-radar observations over rothera (68°s, 68°w) and comparisons with WACCM and eCMAM. *Journal of Atmospheric and Solar-Terrestrial Physics*, *212*, 105510. Retrieved from `https://doi.org/10.1016/j.jastp.2020.105510` doi: 10.1016/j.jastp.2020.105510

Ekanayake, E., Aso, T., & Miyahara, S. (1997, March). Background wind effect on propagation of nonmigrating diurnal tides in the middle atmosphere. *Journal of Atmospheric and Solar-Terrestrial Physics*, *59*(4), 401–429. Retrieved from `https://doi.org/10.1016/s1364-6826(96)00012-0` doi: 10.1016/s1364-6826(96)00012-0

Fiedler, J., Baumgarten, G., & von Cossart, G. (2005, June). Mean diurnal variations of noctilucent clouds during 7 years of lidar observations at ALOMAR. *Annales Geophysicae*, *23*(4), 1175–1181. Retrieved from `https://doi.org/10.5194/angeo-23-1175-2005` doi: 10.5194/angeo-23-1175-2005

Forbes, J. M., Zhang, X., Palo, S., Russell, J., Mertens, C. J., & Mlynczak, M. (2008, February). Tidal variability in the ionospheric dynamo region. *Journal of Geophysical Research: Space Physics*, *113*(A2), n/a–n/a. Retrieved from `https://doi.org/10.1029/2007ja012737` doi: 10.1029/2007ja012737

Fritts, D. C., & Alexander, M. J. (2003, March). Gravity wave dynamics and effects in the middle atmosphere. *Reviews of Geophysics*, *41*(1). Retrieved from `https://doi.org/10.1029/2001rg000106` doi: 10.1029/2001rg000106

Gan, Q., Du, J., Fomichev, V. I., Ward, W. E., Beagley, S. R., Zhang, S., & Yue, J. (2017, April). Temperature responses to the 11 year solar cycle in the mesosphere from the 31 year (1979–2010) extended canadian middle atmosphere model simulations and a comparison with the 14 year (2002–2015) TIMED/SABER observations. *Journal of Geophysical Research: Space Physics*, *122*(4), 4801–4818. Retrieved from `https://doi.org/10.1002/2016ja023564` doi: 10.1002/2016ja023564

Greisiger, K., Schminder, R., & Kürschner, D. (1987, March). Long-period variations of wind parameters in the mesopause region and the solar cycle dependence. *Journal of Atmospheric and Terrestrial Physics*, *49*(3), 281–285. Retrieved from `https://doi.org/10.1016/0021-9169(87)90063-8` doi:

10.1016/0021-9169(87)90063-8

Guharay, A., Batista, P., & Andrioli, V. (2019, October). Investigation of solar cycle dependence of the tides in the low latitude MLT using meteor radar observations. *Journal of Atmospheric and Solar-Terrestrial Physics*, *193*, 105083. Retrieved from `https://doi.org/10.1016/j.jastp.2019.105083` doi: 10.1016/j.jastp.2019.105083

Hibbins, R., Espy, P., Jarvis, M., Riggin, D., & Fritts, D. (2007, April). A climatology of tides and gravity wave variance in the MLT above Rothera, Antarctica obtained by MF radar. *Journal of Atmospheric and Solar-Terrestrial Physics*, *69*(4-5), 578–588. Retrieved from `https://doi.org/10.1016/j.jastp.2006.10.009` doi: 10.1016/j.jastp.2006.10.009

Hibbins, R., Marsh, O., McDonald, A., & Jarvis, M. (2010, June). Interannual variability of the s=1 and s=2 components of the semidiurnal tide in the antarctic MLT. *Journal of Atmospheric and Solar-Terrestrial Physics*, *72*(9-10), 794–800. Retrieved from `https://doi.org/10.1016/j.jastp.2010.03.026` doi: 10.1016/j.jastp.2010.03.026

Hibbins, R. E., Espy, P. J., Orsolini, Y. J., Limpasuvan, V., & Barnes, R. J. (2019, May). SuperDARN observations of semidiurnal tidal variability in the MLT and the response to sudden stratospheric warming events. *Journal of Geophysical Research: Atmospheres*, *124*(9), 4862–4872. Retrieved from `https://doi.org/10.1029/2018jd030157` doi: 10.1029/2018jd030157

Hindley, N. P., Cobbett, N., Fritts, D. C., Janchez, D., Mitchell, N. J., Moffat-Griffin, T., … Wright, C. J. (2021, December). Radar observations of winds, waves and tides in the mesosphere and lower thermosphere over south georgia island (54°s, 36°w) and comparison to WACCM simulations. *ACP*. Retrieved from `https://doi.org/10.5194/acp-2021-981` doi: 10.5194/acp-2021-981

Hines, C., Adams, G., Brosnahan, J., Djuth, F., Sulzer, M., Tepley, C., & Baelen, J. V. (1993, March). Multi-instrument observations of mesospheric motions over arecibo: comparisons and interpretations. *Journal of Atmospheric and Terrestrial Physics*, *55*(3), 241–287. Retrieved from `https://doi.org/10.1016/0021-9169(93)90069-b` doi: 10.1016/0021-9169(93)90069-b

Hocking, W., Fuller, B., & Vandepeer, B. (2001, January). Real-time determination of meteor-related parameters utilizing modern digital technology. *Journal of Atmospheric and Solar-Terrestrial Physics*, *63*(2-3), 155–169. Retrieved from `https://doi.org/10.1016/s1364-6826(00)00138-3` doi: 10.1016/s1364-6826(00)00138-3

Jacobi, C., Schminder, R., Kürschner, D., Bremer, J., Greisiger, K., Hoffmann, P., & Singer, W. (1997, January). Long-term trends in the mesopause wind field obtained from LF d1 wind measurements at collm, germany. *Advances in Space Research*, *20*(11), 2085–2088. Retrieved from `https://doi.org/10.1016/s0273-1177(97)00599-1` doi: 10.1016/s0273-1177(97)00599-1

Kalnins, A. (2018, May). Multicollinearity: How common factors cause type 1 errors in multivariate regression. *Strategic Management Journal*, *39*(8), 2362–2385. Retrieved from `https://doi.org/10.1002/smj.2783` doi: 10.1002/smj.2783

Laskar, F. I., Chau, J. L., Stober, G., Hoffmann, P., Hall, C. M., & Tsutsumi, M. (2016, May). Quasi-biennial oscillation modulation of the middle- and high-latitude mesospheric semidiurnal tides during august-september. *Journal of Geophysical Research: Space Physics*, *121*(5), 4869–4879. Retrieved from `https://doi.org/10.1002/2015ja022065` doi: 10.1002/2015ja022065

Lee, D. Y., Petersen, M. R., & Lin, W. (2019, December). The southern annular mode and southern ocean surface westerly winds in e3sm. *Earth and Space Science*, *6*(12), 2624–2643. Retrieved from `https://doi.org/10.1029/2019ea000663` doi: 10.1029/2019ea000663

Lieberman, R. S., Riggin, D. M., Ortland, D. A., Nesbitt, S. W., & Vincent, R. A. (2007, October). Variability of mesospheric diurnal tides and tropospheric diurnal heating during 1997–1998. *Journal of Geophysical Research*, *112*(D20). Retrieved from https://doi.org/10.1029/2007jd008578 doi: 10.1029/2007jd008578

Liu, G., Lieberman, R. S., Harvey, V. L., Pedatella, N. M., Oberheide, J., Hibbins, R. E., ... Janches, D. (2021, March). Tidal variations in the mesosphere and lower thermosphere before, during, and after the 2009 sudden stratospheric warming. *Journal of Geophysical Research: Space Physics*, *126*(3). Retrieved from https://doi.org/10.1029/2020ja028827 doi: 10.1029/2020ja028827

Liu, H., Sun, Y.-Y., Miyoshi, Y., & Jin, H. (2017, May). ENSO effects on MLT diurnal tides: A 21 year reanalysis data-driven GAIA model simulation. *Journal of Geophysical Research: Space Physics*, *122*(5), 5539–5549. Retrieved from https://doi.org/10.1002/2017ja024011 doi: 10.1002/2017ja024011

Manson, A. H., Meek, C. E., Hall, C. M., Nozawa, S., Mitchell, N. J., Pancheva, D., ... Hoffmann, P. (2004, January). Mesopause dynamics from the scandinavian triangle of radars within the PSMOS-DATAR project. *Annales Geophysicae*, *22*(2), 367–386. Retrieved from https://doi.org/10.5194/angeo-22-367-2004 doi: 10.5194/angeo-22-367-2004

Marshall, G. J. (2003, December). Trends in the southern annular mode from observations and reanalyses. *Journal of Climate*, *16*(24), 4134–4143. Retrieved from https://doi.org/10.1175/1520-0442(2003)016<4134:titsam>2.0.co;2 doi: 10.1175/1520-0442(2003)016⟨4134:titsam⟩2.0.co;2

Mayr, H. G. (2005). Interannual variations of the diurnal tide in the mesosphere generated by the quasi-biennial oscillation. *Journal of Geophysical Research*, *110*(D10). Retrieved from https://doi.org/10.1029/2004jd005055 doi: 10.1029/2004jd005055

McLandress, C., & Ward, W. E. (1994). Tidal/gravity wave interactions and their influence on the large-scale dynamics of the middle atmosphere: Model results. *Journal of Geophysical Research*, *99*(D4), 8139. Retrieved from https://doi.org/10.1029/94jd00486 doi: 10.1029/94jd00486

Merzlyakov, E., Murphy, D., Vincent, R., & Portnyagin, Y. (2009, January). Long-term tendencies in the MLT prevailing winds and tides over antarctica as observed by radars at molodezhnaya, mawson and davis. *Journal of Atmospheric and Solar-Terrestrial Physics*, *71*(1), 21–32. Retrieved from https://doi.org/10.1016/j.jastp.2008.09.024 doi: 10.1016/j.jastp.2008.09.024

Mitchell, N. J. (2002). Mean winds and tides in the arctic mesosphere and lower thermosphere. *Journal of Geophysical Research*, *107*(A1). Retrieved from https://doi.org/10.1029/2001ja900127 doi: 10.1029/2001ja900127

Namboothiri, S., Manson, A., & Meek, C. (1993, August). Variations of mean winds and tides in the upper middle atmosphere over a solar cycle, saskatoon, canada, 52°n, 107°w. *Journal of Atmospheric and Terrestrial Physics*, *55*(10), 1325–1334. Retrieved from https://doi.org/10.1016/0021-9169(93)90101-4 doi: 10.1016/0021-9169(93)90101-4

Pancheva, D., Mukhtarov, P., & Andonov, B. (2009, February). Global structure, seasonal and interannual variability of the migrating semidiurnal tide seen in the SABER/TIMED temperatures (2002–2007). *Annales Geophysicae*, *27*(2), 687–703. Retrieved from https://doi.org/10.5194/angeo-27-687-2009 doi: 10.5194/angeo-27-687-2009

Pancheva, D. V., Mukhtarov, P. J., Shepherd, M. G., Mitchell, N. J., Fritts, D. C., Riggin, D. M., ... Kikuchi, T. (2006). Two-day wave coupling of the low-latitude atmosphere-ionosphere system. *Journal of Geophysical Research*, *111*(A7). Retrieved from https://doi.org/10.1029/2005ja011562 doi: 10.1029/2005ja011562

Pedatella, N. M., & Liu, H.-L. (2012, October). Tidal variability in the mesosphere and lower thermosphere due to the el niño-southern oscillation. *Geophysical Research Letters*, *39*(19), n/a–n/a. Retrieved from https://doi.org/

10.1029/2012gl053383 doi: 10.1029/2012gl053383

Pedatella, N. M., Richter, J. H., Edwards, J., & Glanville, A. A. (2021, August). Predictability of the mesosphere and lower thermosphere during major sudden stratospheric warmings. *Geophysical Research Letters*, *48*(15). Retrieved from https://doi.org/10.1029/2021gl093716 doi: 10.1029/2021gl093716

Ramesh, K., Smith, A. K., Garcia, R. R., Marsh, D. R., Sridharan, S., & Kumar, K. K. (2020, December). Long-term variability and tendencies in migrating diurnal tide from WACCM6 simulations during 1850–2014. *Journal of Geophysical Research: Atmospheres*, *125*(23). Retrieved from https://doi.org/10.1029/2020jd033644 doi: 10.1029/2020jd033644

Sassi, F. (2004). Effect of el niño–southern oscillation on the dynamical, thermal, and chemical structure of the middle atmosphere. *Journal of Geophysical Research*, *109*(D17). Retrieved from https://doi.org/10.1029/2003jd004434 doi: 10.1029/2003jd004434

Smith, A. K. (2012, June). Global dynamics of the MLT. *Surveys in Geophysics*, *33*(6), 1177–1230. Retrieved from https://doi.org/10.1007/s10712-012-9196-9 doi: 10.1007/s10712-012-9196-9

Sprenger, K., & Schminder, R. (1969, January). Solar cycle dependence of winds in the lower ionosphere. *Journal of Atmospheric and Terrestrial Physics*, *31*(1), 217–221. Retrieved from https://doi.org/10.1016/0021-9169(69)90100-7 doi: 10.1016/0021-9169(69)90100-7

Stober, G., Janches, D., Matthias, V., Fritts, D., Marino, J., Moffat-Griffin, T., … Palo, S. (2021, January). Seasonal evolution of winds, atmospheric tides, and reynolds stress components in the southern hemisphere mesosphere–lower thermosphere in 2019. *Annales Geophysicae*, *39*(1), 1–29. Retrieved from https://doi.org/10.5194/angeo-39-1-2021 doi: 10.5194/angeo-39-1-2021

Stober, G., Kuchar, A., Pokhotelov, D., Liu, H., Liu, H.-L., Schmidt, H., … Mitchell, N. (2021, September). Interhemispheric differences of mesosphere–lower thermosphere winds and tides investigated from three whole-atmosphere models and meteor radar observations. *Atmospheric Chemistry and Physics*, *21*(18), 13855–13902. Retrieved from https://doi.org/10.5194/acp-21-13855-2021 doi: 10.5194/acp-21-13855-2021

Sundararajan, S. (2020, June). Equatorial upper mesospheric mean winds and tidal response to strong el niño and la niña. *Journal of Atmospheric and Solar-Terrestrial Physics*, *202*, 105270. Retrieved from https://doi.org/10.1016/j.jastp.2020.105270 doi: 10.1016/j.jastp.2020.105270

Teitelbaum, H., & Vial, F. (1991, August). On tidal variability induced by nonlinear interaction with planetary waves. *Journal of Geophysical Research: Space Physics*, *96*(A8), 14169–14178. Retrieved from https://doi.org/10.1029/91ja01019 doi: 10.1029/91ja01019

Trenberth, K. (2021, Jan). *Nino sst indices (nino 1 2, 3, 3.4, 4; oni and tni).* National Center for Atmospheric Research. Retrieved from https://climatedataguide.ucar.edu/climate-data/nino-sst-indices-nino-12-3-34-4-oni-and-tni

Trenberth, K. E. (2002). Evolution of el niño–southern oscillation and global atmospheric surface temperatures. *Journal of Geophysical Research*, *107*(D8). Retrieved from https://doi.org/10.1029/2000jd000298 doi: 10.1029/2000jd000298

Vial, F., Lott, F., & Teitelbaum, H. (1994, July). A possible signal of the el niño-southern oscillation in time series of the diurnal tide. *Geophysical Research Letters*, *21*(15), 1603–1606. Retrieved from https://doi.org/10.1029/94gl01016 doi: 10.1029/94gl01016

Webster, A. (2012). *Introductory regression analysis : With computer application for business and economics.* London: Taylor & Francis Group.

Wilhelm, S., Stober, G., & Chau, J. L. (2017, July). A comparison of 11-year mesospheric and lower thermospheric winds determined by meteor and MF radar at 69 N. *Annales Geophysicae*, *35*(4), 893–906. Retrieved from https://doi.org/10.5194/angeo-35-893-2017 doi: 10.5194/angeo-35-893-2017

Xu, J., Smith, A. K., Liu, H.-L., Yuan, W., Wu, Q., Jiang, G., ... Franke, S. J. (2009, July). Seasonal and quasi-biennial variations in the migrating diurnal tide observed by thermosphere, ionosphere, mesosphere, energetics and dynamics (TIMED). *Journal of Geophysical Research*, *114*(D13). Retrieved from https://doi.org/10.1029/2008jd011298 doi: 10.1029/2008jd011298

Yiğit, E., & Medvedev, A. S. (2015, February). Internal wave coupling processes in earth's atmosphere. *Advances in Space Research*, *55*(4), 983–1003. Retrieved from https://doi.org/10.1016/j.asr.2014.11.020 doi: 10.1016/j.asr.2014.11.020

Yiğit, E., Medvedev, A. S., & Ern, M. (2021, February). Effects of latitude-dependent gravity wave source variations on the middle and upper atmosphere. *Frontiers in Astronomy and Space Sciences*, *7*. Retrieved from https://doi.org/10.3389/fspas.2020.614018 doi: 10.3389/fspas.2020.614018